EXPERIMENTAL STUDY OF THE STABILITY OF THE BOUNDARY LAYER OVER A ROTATING DISK, WITH VISCOSITY VARIATIONS IN THE BOUNDARY LAYER

José Pontes
Metallurgy and Materials Engineering Department – EE/COPPE/UFRJ
PO Box 68505, 21945-970 Rio de Janeiro RJ, Brazil
jopontes@ufrj.br

Norberto Mangiavacchi
Department of Mechanical Engineering – State Unversity of Rio de Janeiro - UERJ
20550-013 - Rio de Janeiro RJ, Brazil
norberto@uerj.br

Mila R. Avelino
Department of Mechanical Engineering – State Unversity of Rio de Janeiro - UERJ
20550-013 - Rio de Janeiro RJ, Brazil
mila@uerj.br

Gustaf Akerman
Mechanical Engineering Laboratory– State Unversity of Rio de Janeiro - UERJ
20550-013 - Rio de Janeiro RJ, Brazil
akerman@uerj.br

Michelle Bastos
Department of Mechanical Engineering – State Unversity of Rio de Janeiro - UERJ
20550-013 - Rio de Janeiro RJ, Brazil
milly.bastos@ig.com.br

Abstract. *T*he boundary layer in the vicinity of a rotating disk is very similar to the boundary layer over a swept wing, and has received much attention as a prototype of three-dimensional boundary layers for the study of cross-flow instabilities. Pontes et al (2002) have predicted analytically that the stability of infinitesimal perturbations in this boundary layer is affected by the presence of a viscous gradient in the proximity of the disk. For instance, the neutral Reynolds number for stationary disturbances is substantially reduced if the viscosity increases close the wall. An experimental apparatus specially designed to simulate the stability of a boundary layer over a rotating disk is described here in detail. The effects in the boundary layer due to the viscosity variation are also presented. In this work a visualization technique is employed in an experimental apparatus to experimentally corroborate the effect of variations in the viscosity profile in the boundary layer over the rotating disk. The viscosity in the boundary layer is increased by cooling the disk, keeping the surface temperature constant. Measurements obtained in the apparatus are consistent with results obtained in the analysis, showing that finite amplitude stationary disturbances follow the trend found in the analysis of infinitesimal disturbances.

Keywords: *Rotating Disk Flow, Hydrodynamic Stability, Turbulence, Experimental Methods*

1. Introduction

Boundary layers developed close to the axis of rotating disks have long been used as a prototype for stability and transition studies on three-dimensional flows, as those observed in swept-wings of modern airplanes. In swept wings, the flow may be decomposed in a primary one, parallel to the airfoil chord, and a secondary cross-flow, perpendicular to the chord, which is thought to be responsible for the early onset of transition. Since 60% of the drag on an airplane in flight is due to skin-friction (Lingwood, 1995), considerable efforts have been made over the last 20 years, aiming to stabilize the boundary layer, and increase the area over which the flow is laminar, rather than turbulent.

As sketched in Fig. 1, rotating disk flow presents certain simplifications and advantages over the swept-wing problem, which makes the study on stability easier to be handled (Lingwood, 1995): the flow does not have a pressure gradient along the radial direction, controlling the experimental conditions is relatively simple, besides there is an exact similarity solution of the Navier-Stokes equations for the laminar stationary flow, where the velocity profiles are independent of the radius and the boundary layer thickness is constant along the radial direction (Von Kármán, 1921, Schlichting, 2000). In addition, rotating disk flow presents inflectional laminar profiles, which may trigger the instability. The major difference between these flows is that the Coriolis forces are not present in the velocity field over swept-wings.

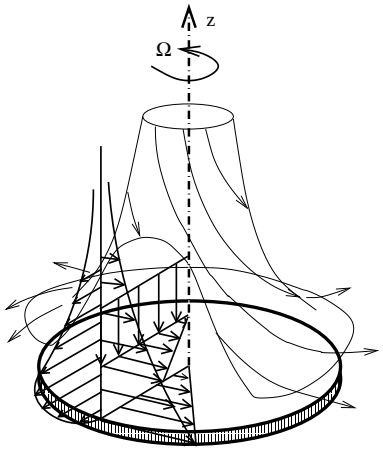

Fig. 1: Rotating Disk Flow

Rotating disk flow instabilities appear in the form of corotating vortices which spiral outward with their axes along logarithmic spirals. The first study of transition on a rotating disk is due to Smith (1946). Subsequently, Gregory, Stuart & Walker (1955) found stationary vortices from a non-dimensional radius $R = 430$ in a flow visualization by using the wet-china-clay technique, and first discussed the application to swept-back airfoils.

Malik (1986) determined the neutral stability curve for stationary vortex disturbances, which turn with same angular velocity of the disk. Faller (1991) determined the neutral stability curves for setup configurations consisting of rotating or stationary disks and flows approaching the disk with (rotating flow) or without (stationary flow) bulk angular velocity. Lingwood (1995) presented the neutral curve for vortices turning with several angular velocities and theoretical results concerning the asymptotic response of the flow to an impulsive excitation exerted in the flow at a certain radius in $t = 0$. Additionally, Lingwood's work addresses the case where the wavenumber component along the radial direction is complex, leading to an exponential growth along that direction. The curve for this case defines the region of absolute instability.

Rotating disk flow is also used as a model flow in the study of polarization curves experimentally obtained in electro-chemical cells. A typical setup used in the study of electro-dissolution of iron electrodes in a 1 **M H_2SO_4** solution is shown in Fig. 2. The working electrode consists of an iron cylindrical rod, coated with a resin, except in a small disk at the base, through which the electric current flows to the electrolyte. The rod is driven by a variable velocity electric motor. Polarization curves experimentally obtained with this setup present a current instability, schematically shown in Fig. 2, which may be due to an instability in the hydrodynamic field developed close to electrode base.

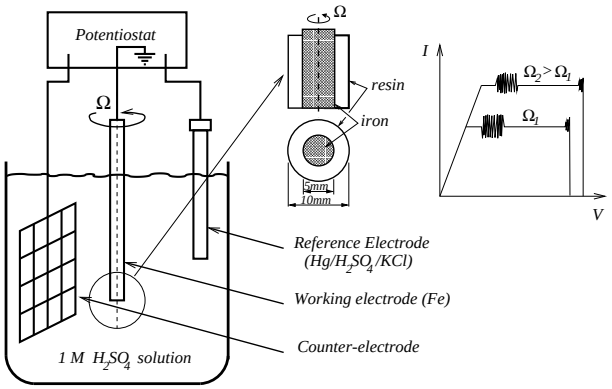

Fig. 2: The electro-chemical cell using a rotating disk electrode

The stability of the hydrodynamic field is affected by the process of electro-dissolution of the iron electrode, which leads to the existence of a concentration field of chemical species, and to an axial viscosity gradient in the diffusion boundary layer (Barcia et al. 1992, Ferreira, 1994). Pontes *et. al* (2002) showed that the steady flow, affected by the viscosity gradient was less stable than the classical one, with respect to disturbances with periodic variation along the radial direction. On three subsequent papers, Pontes *et al.* (2002a, 2002b, 2003) further indicated that the flow affected by the viscosity gradient was, in many cases, less stable to spiral disturbances, periodically varying along the radial and azimuthal directions, than the constant viscosity flow studied by Malik (1986) and Lingwood (1995).

One of the purposes of this paper is to present in detail, the parameters adopted to design an apparatus capable of

experimentally simulate the the stability of a boundary layer over a rotating disk. The experimental setup is currently under construction at the Department of Mechanical Engineering of the State University of Rio de Janeiro, and is intended to be used as a complementary setup to the one used for electro-chemical experiments at the Metallurgy and Materials Engineering of the Federal University of Rio de Janeiro.

This complementary setup will provide experimental corroboration of the unstabilizing effect of a viscosity profile in the normal direction to the rotating disk. A viscosity increase in the region close to the disk wall will be introduced by cooling the disk surface, thus introducing a temperature gradient in the boundary layer. The viscosity and velocity profiles thus obtained are not necessarily identical to the case of a viscosity introduced by chemical species concentration gradients, however the thermal problems is itself interesting, it is mathematically simpler, and it provides a good first approximation to the chemical problem.

The paper is organized as follows: Section (2) describes the steady velocity flow, which is the problem base state, for the case of constant viscosity fluids and for one variable viscosity configuration. Section (3) details the setup specially designed and built to simulate the geometry of interest. The design criteria and the construction procedures are also presented. Section (4) describes the instrumentation of the setup. Section (5) furnishes the experimental procedures that will be employed during the experiments, in Section (6) the experimental results are presented, and Sec. (7) concludes the work.

2. The Base State

The steady hydrodynamic field is the well known Von Kármán (1921) exact solution of the continuity and Navier-Stokes equations for laminar rotating disk-flow, written in a rotating coordinate frame turning with the disk angular velocity Ω:

$$\mathbf{div}\,\mathbf{v} = 0 \tag{1}$$

$$\frac{D\mathbf{v}}{Dt} = -2\Omega \times \mathbf{v} - \frac{1}{\rho}\,\mathbf{grad}\,p + \frac{1}{\rho}\,\mathbf{div}\,\tau \tag{2}$$

where $-2\Omega \times \mathbf{v} = 2\Omega\,(v_\theta \mathbf{e}_r - v_r \mathbf{e}_\theta)$ and τ is the viscous stress tensor for a Newtonian fluid with the viscosity μ depending on the axial coordinate z. The components of stress tensor are given by (Schlichting, 1968):

$$\left.\begin{aligned} \tau_{rr} &= 2\mu\frac{\partial v_r}{\partial r} & \tau_{r\theta} &= \tau_{\theta r} = \mu\left(r\frac{\partial}{\partial r}\left(\frac{v_\theta}{r}\right) + \frac{1}{r}\frac{\partial v_r}{\partial \theta}\right) \\ \tau_{\theta\theta} &= 2\mu\left(\frac{1}{r}\frac{\partial v_\theta}{\partial \theta} + \frac{v_r}{r}\right) & \tau_{\theta z} &= \tau_{z\theta} = \mu\left(\frac{\partial v_\theta}{\partial z} + \frac{1}{r}\frac{\partial v_z}{\partial \theta}\right) \\ \tau_{zz} &= 2\mu\frac{\partial v_z}{\partial z} & \tau_{rz} &= \tau_{zr} = \mu\left(\frac{\partial v_r}{\partial z} + \frac{\partial v_z}{\partial r}\right) \end{aligned}\right\} \tag{3}$$

The steady solution takes the form:

$$\bar{v}_r = r\,\Omega\,F(\xi) \tag{4}$$

$$\bar{v}_\theta = r\,\Omega\,G(\xi) \tag{5}$$

$$\bar{v}_z = (\nu(\infty)\,\Omega)^{1/2}\,H(\xi) \tag{6}$$

$$\bar{p} = \rho\nu(\infty)\Omega P(\xi) \tag{7}$$

where $\xi = z(\Omega/\nu(\infty))^{1/2}$ and $\nu(\infty)$ is the bulk viscosity, far from the electrode surface. Equations (4–7) are introduced in the dimensional continuity and Navier-Stokes equations, leading to the following system of equations for F, G, H and P.

$$2F + H' = 0 \tag{8}$$

$$F^2 - (G+1)^2 + HF' = \frac{\partial}{\partial\xi}\left(\frac{\nu(\xi)}{\nu(\infty)}F'\right) \tag{9}$$

$$2F(G+1) + HG' = \frac{\partial}{\partial\xi}\left(\frac{\nu(\xi)}{\nu(\infty)}G'\right) \tag{10}$$

$$P' + HH' = 2\frac{\nu'(\xi)}{\nu(\infty)}H' + \frac{\nu(\xi)}{\nu(\infty)}H'' \tag{11}$$

Boundary conditions for F, G and H are $F = H = P = G = 0$ when $\xi = 0$, $F = H' = 0$, $G = -1$ when $\xi \longrightarrow \infty$. In order to integrate Eqs. (8–11) a viscosity profile must be assumed. In this work we use the following profile proposed by Barcia *et. al* (1992):

$$\frac{\nu(\xi)}{\nu(\infty)} = \frac{\nu(0)}{\nu(\infty)} + \left(1 - \frac{\nu(0)}{\nu(\infty)}\right)\frac{q^{1/3}}{\Gamma(4/3)}\int_0^\xi e^{-q\xi^3}\,d\xi \tag{12}$$

The parameter q defines the slope of the viscosity profile close to the electrode surface. Figure 6 shows the non-dimensional viscosity and velocity profiles obtained by numerical integration of Eqs. (8–11) and used in the stability

analysis presented in this work. The parameters assumed for the viscosity profile are $\nu(0)/\nu(\infty) = 6$ and $q = 2$.

Variables in Eqs. (1–2) are made non-dimensional as follows: radial and axial coordinates are divided the reference length $(\nu(\infty)/\Omega)^{1/2}$, velocity components are divided by the reference velocity $r_e^*\Omega$, pressure is divided by the reference pressure $\rho r_e^{*}\Omega^2$, viscosity is divided by the bulk value, $\nu^*(\infty)$ and time and the eigenvalue of the linearized problem are made non-dimensional using the factor $\nu(\infty)^{1/2}/(r_e^*\Omega^{3/2})$. Here, r_e^* is the dimensional coordinate along the radial direction where the stability analysis is made. We define also the Reynolds number by the relation:

$$R = r_e^* \left(\frac{\Omega}{\nu(\infty)} \right)^{1/2} \tag{13}$$

3. Experimental setup

To observe the phenomenon of boundary layer instability over a rotating disk an experimental apparatus is then designed and built. The observations on the behavior of the phenomena will corroborate the theoretical results obtained with stability analysis of the hydrodynamic field as formulated in Sec. (2).

This section describes in detail the initial design parameters adopted, and a brief description of the experimental procedures on a rotating disk experimental apparatus. Also, the instrumentation used in the experiments is specified.

3.1. Design of the experimental setup

Geometry and dimensions of the whole apparatus are determined in order to cover most interesting situations during the experiments. Initial design parameters were chosen to provide critical conditions of the phenomenon.

The rotating disk setup, showed in Fig. 3, is composed of a cubic glasstank with a squared $688mm^2$ cross section area and depth of 688mm, mounted on a metal frame. This enclosure houses a disk, 500mm diameter and 30mm thick, placed in a horizontal plane, at 70mm far from the ground and mounted on a vertical drive shaft. The complete disk/vertical drive shaft assembly is immersed in water. Figure 3 shows the general setup in three views. The disk velocity is regulated and held fixed at constant value during each experiment. The drawings were carried out in SolidWorks 3D modeling software.

Figure 4. including the AC motor, the disk shaft mounted vertically on the shaft driven by an AC motor with a pulley-belt transmission, as can be seen in the figures.

The bearing is a nylon-Teflon plug inserted at the bottom of the tank as seen in figures 4 and 5.

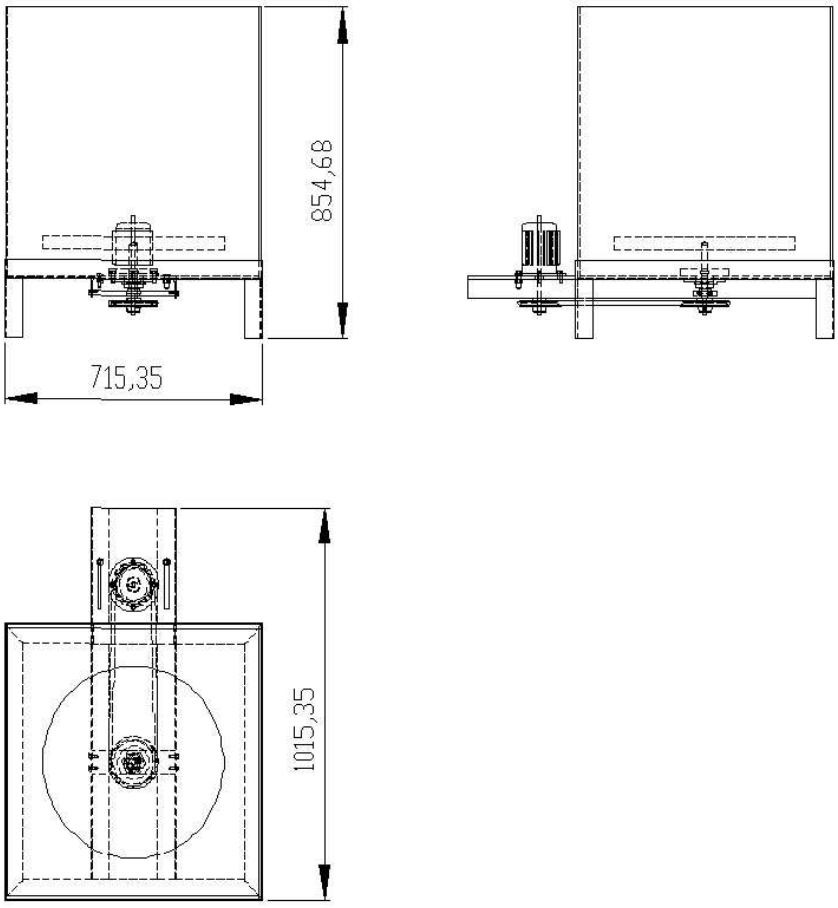

Fig. 3: Sketch of the apparatus, 3 views.

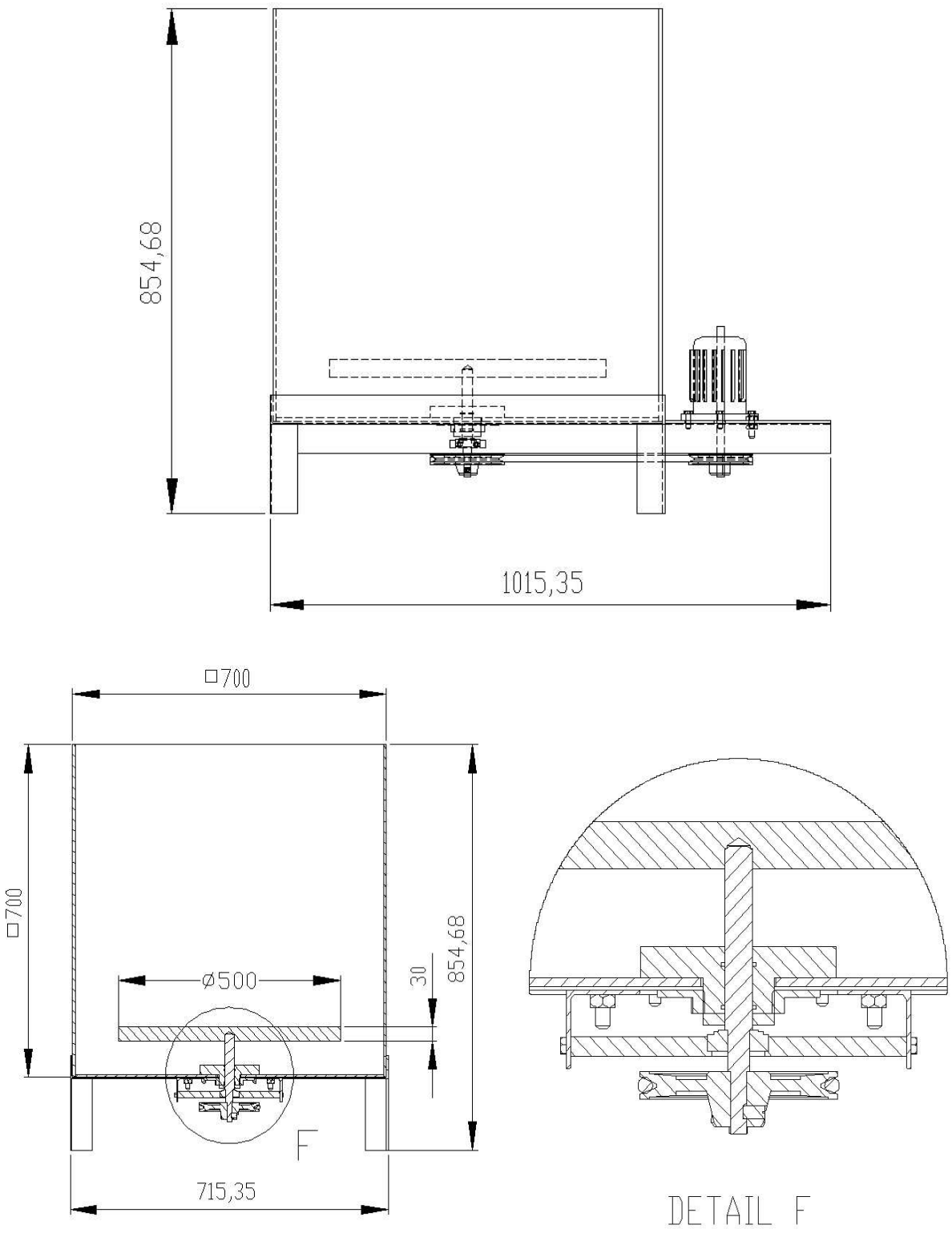

Fig. 4: Sketch of the apparatus, bearing, and pulley-belt transmission.

3.2. Experimental Setup Construction

The tank was constructed with 6mm glass plates, mounted on a steel frame in order to allow visualization from various angles. The drive shaft is inserted across the bottom of the tank and is driven by a 1/8 hp, 1720 rpm motor through a belt and pulley speed system. A pulley set with 135 mm, 115 mm, 90 mm, 65 mm and 40 mm diameter could be used to obtain diferent speeds. A nylon plug with rubber rings was used to stop up water in the passage of the shaft in the bottom of the tank. To annul any deviation that could be caused by the belt system and pulley in the vertical position of the shaft, a roller of conical rolls was used.

Various disks were fabricated, with different objectives. A solid acrylic disk was fabricated for visualization purposes. A aluminum-alloy disk, with an internal chamber, was constructed to perform thermal experiments. Other disks where constructed, with various inserts over the surface, to introduce perturbations in the velocity field. The disks work as a flywheels that store energy, thus reducing velocity variations. Each disk was treated, either machined ou polished to come as close as possible to a smooth surface. The roughness of the disk surface depend on the disk in use. In order to comply with the axisymmetrical condition of the flow, the disk could have been placed in the median plane of a bottomless cylinder, with bigger diameter and higher from the bottom of the tank in such a way that the water above the disk may be consider as infinite. This movable device would work as a cover and the distance from the rotating disk should be considered as sufficiently large in relation to the thickness of the boundary layer.

In order to refrigerate the disk, an ice compartment was build under the disk, as showh in figure 5.

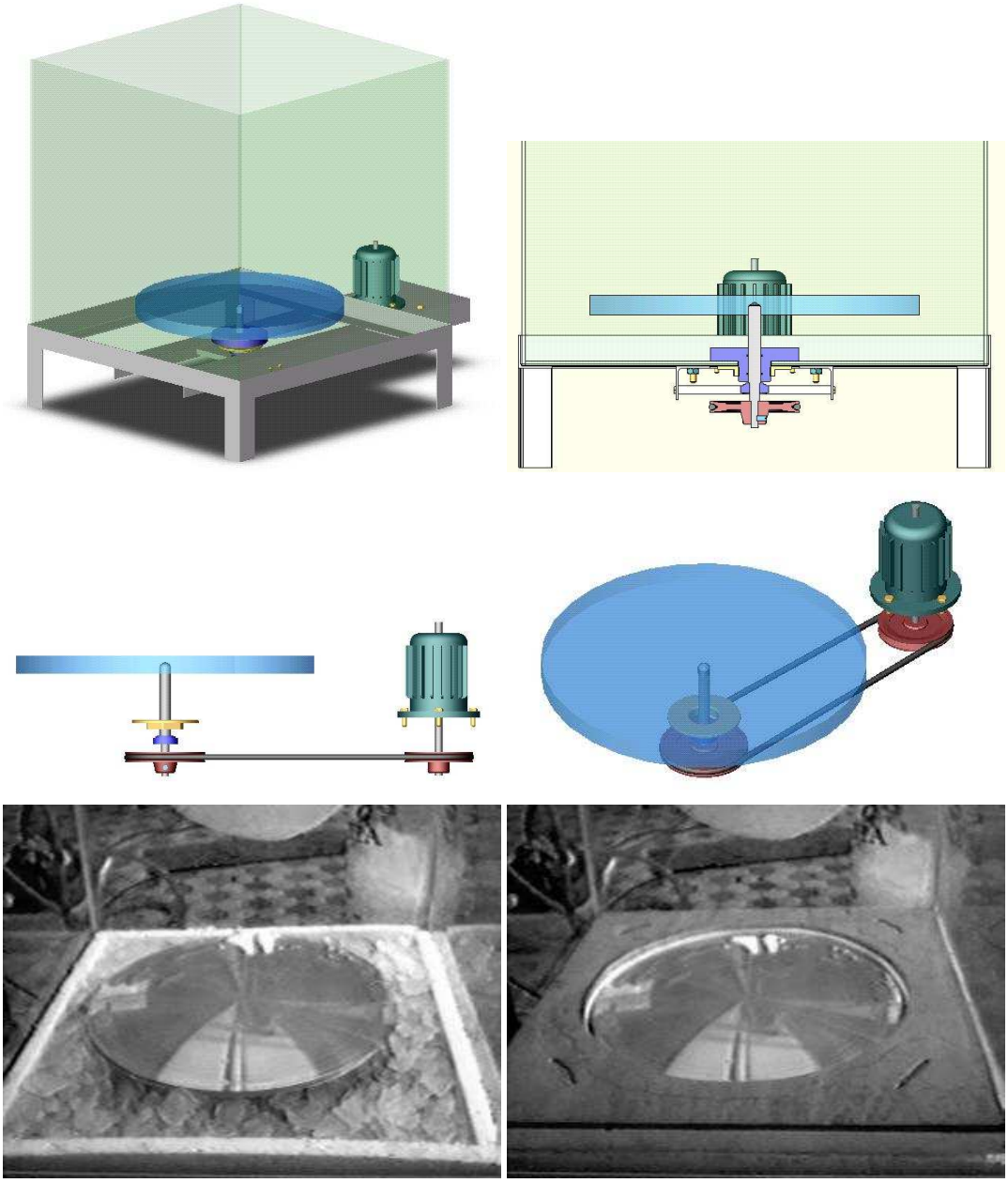

Fig. 5: General view of the experimental setup. 3D rendering (top), and detail of the assembly of the refrigeration system (botton).

4. Instrumentation

The instrumentation is responsible for the control of the rotation of the disk, the positioning system for the sensors, and the data acquisition. While some of the measurements are performed by reading instruments and writing down the values by hand, we implement automatized data acquisition and control in the most demanding tasks. A cost-efficient PC-based data acquisition (DAQ) and control system was implemented using hardware and software from National Instruments.

1. Velocity measurements
   - Pitot tube: average velocity measurements are obtained using a 2mm Pitot tube, connected to a inclined water column micro-manometer, allowing accurate velocity measurements down to 0.1m/s.
   - Hot-film anemometer: Velocity measurements in the boundary layer are performed with hot-film probe fitted to the end of a probe support tube connected to a vertical traveler positioning system. With help of the positioning traveler gear, the probe is moved vertically. Using a screw system, the positioning system is 0.25mm accurate. The probe fitted to a mobile carriage settled in the traveler gear positioning system can be moved in one horizontal plane parallel to the edges of the tank. Each movement is controlled by a 1/4mm graduated rule allocated at the positioning system. A National Instruments data conditioning and acquisition board is employed. The signals are processed using LabVIEW, in a PC running RedHat Linux 9.0.
2. Temperature measurement using Thermocouple thermometers: temperature measurements in the boundary layer are obtained using thermocouple thermometers, connected to a National Instruments data acquisition board, and LabVIEW.
3. Motor rotation control: using a solid state frequency controller, with set point control provided by the PC.
4. Sensors positioning system: The traveler gear is a, 2 DOF positioning system shown in the figure 5. Using a screw system, the positioning system is 0.25mm accurate. The mechanical system, however, is ready to be driven by step-motors, and to be integrated into the automated system.
5. Pressure transducers: Differential pressure measurements are mostly performed using U-type micro-manometers, and the readings are currently performed manually. Pressure transducers may eventually substitute these micro-manometers and provide continuous logging of experimental pressure data.

5. Experiments

The disk's flatness is checked beforehand, and the precision of the probe in relation to the complete disk surface is 1.0 millimeter during the rotation.

When the experiment was operating, the sensitive element of the probe was placed at a distance of 1.0mm from the disk surface, parallel to the disk surface. This high was chosen because of the dimensions of the sensor, to avoid interference to the sensor in the flow, by approximating the sensor to the wall. The experimental study concerning measurements of velocity and temperature.

Four different experimental simulations are performed: base velocity profile measurements (Pitot tube), temperature profile/fluctuation measurements (thermocouples), velocity fluctuations measurements (hot wire anemometer), and visualization experiments. For each type of experiment a different selection of experimental conditions is chosen, as shown in table 1. In these experiments the rotation velocity is kept mostly constant, since lower disk velocities imply in lower pressure readings, and therefore, less accurate velocity readings.

Table 1. Parameters selection for the experiments.

Experiment	Fluid	Viscosity	Rotation speed	Reynolds Number	δ
1	glycerin	$1 \times 10^{-3} s$	$10 s^{-1}$	25	6×10^{-2}
1	glycerin and water	$1 \times 10^{-4} s$	$1 s^{-1}$	25	6×10^{-2}
2	glycerin and water	$1 \times 10^{-4} s$	$10 s^{-1}$	75	2×10^{-2}
3	glycerin and water	$1 \times 10^{-5} s$	$10 s^{-1}$	250	6×10^{-3}
4	water	$1 \times 10^{-6} s$	$10 s^{-1}$	750	2×10^{-3}
4	water	$1 \times 10^{-6} s$	$1 s^{-1}$	250	6×10^{-3}

1. Mean velocity measurements: These measurements are obtained with the Pitot tube, hence it is desirable that the boundary layer is as thick as possible, while still maintaining a relatively high disk speed. The parameters are chosen such that the boundary layer thickness is $\delta = 6 \times 10^{-2} m$. This requires either employing glycerine as the working fluid, and/or decreasing the rotation speed as much as possible.
2. Temperature measurements: For this kind of experiments a thick boundary layer is desirable, such that it is possible to obtain, at least, a coarse mesh temperature profile. However, as we require relatively high Reynolds numbers, we choose a boundary layer with $\delta = 2 \times 10^{-2} m$.
3. Velocity fluctuation experiments: These experiments allow to analyze in mode detail the propagation of perturbations in the boundary layer. Measurements are performed with hot wire anemometers, which allow to make measurements fairly close to the disk wall. However, in this case, a too thin boundary layer may reduce the accuracy of the measurements. A boundary layer thickness of $6 \times 10^{-3} m$ is considered adequate for this kind of experiments.
4. Visualization experiments: These experiments are mainly intended to determine the region (and therefore the Reynolds number) at which perturbations are first observable. For these visualizations it is not necessary to have a very thick boundary layer, as perturbations in the velocity profile can be observed by means of tracer injection even if the hydrodynamic boundary layer is only a few millimeters thick. The dye is methylene blue, and it moves outward in the boundary layer after being poured in at the center of the disk to visualize the perturbations. It is

desirable, in this case, to be able to reach Reynolds numbers in the range of 500, to reach the turbulent transition. Experiments can, therefore, be performed using water. Varying the rotation speed, it is possible do change the radial position on the disk where instabilities are first observed.

6. Results

The purpose of this work is to perform an experimental investigation on the effect of perturbation imposed to a given viscosity profile, on the disturbances in rotating disk flow with a steady viscosity profile.

First, we validated experimentally the velocity profiles obtained by Pontes *et al.* (2002b, 2003), obtained with Eq.(12). Figure 6 shows the velocity profiles computed from Eq.(12). Values measured experimentally are in qualitative agreement with the values obtained numerically.

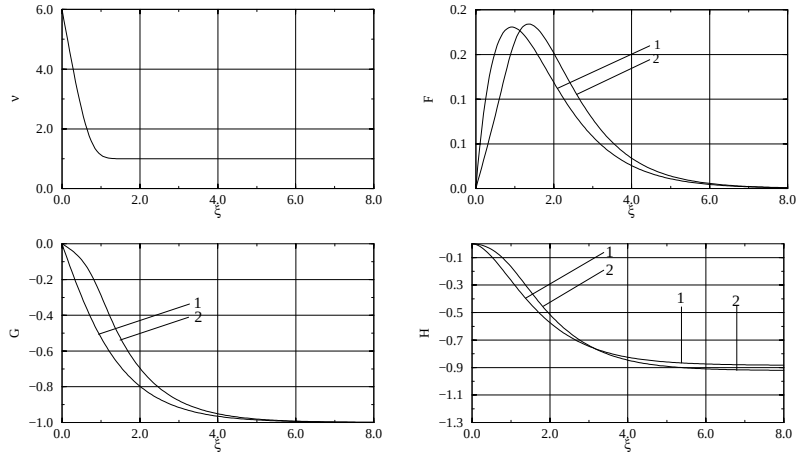

Fig. 6: Dimensionless viscosity, ν, and velocity profiles F, G and H. Curves No. 1 refer to constant viscosity fluids. Curves No. 2: variable viscosity fluids with $\nu(0)/\nu(\infty) = 6$ and $q = 2$ (see Eq. 12).

We turn now to the experimental results obtained using the visualization technique described above. One typical result obtained with this technique is presented in Fig. 7,

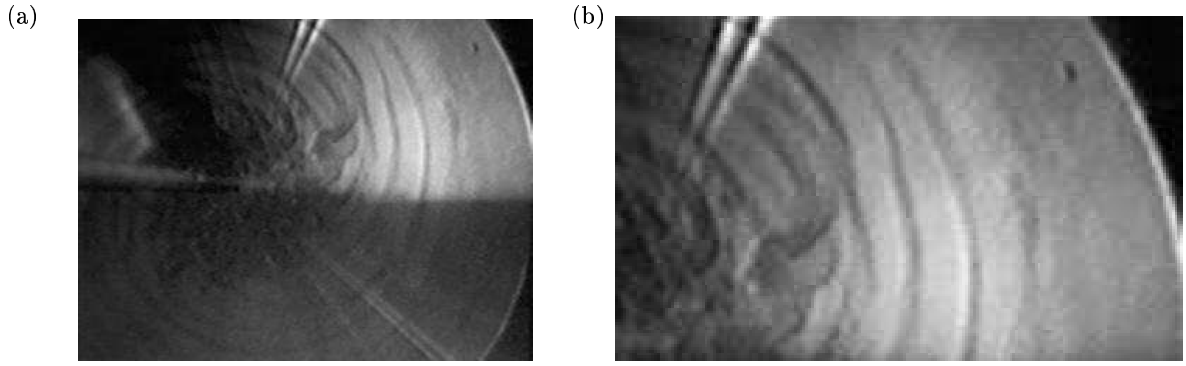

Fig. 7: Visualization experiment, intended to determine the region (and therefore the Reynolds number) at which perturbations are first observable. Isothermal experiment, General view (left) and detail (right). Data for this experiment were: $T_\infty = 20C$, $\Omega = 5.12rad/s$, $\nu = 1.00 \times 10^{-6} m^2/s$, $r_c = 0.168m$, hence $R_c = 380$. For the case of the Refrigerated disk, data were: $T_\infty = 15C$, $\Omega = 4.40rad/s$, $\nu = 1.138 \times 10^{-6} m^2/s$, $r_c = 0.171m$, hence $R_c = 336$.

The pictures in figure 7 show the helical lines that develop from the point of injection being dispersed by perturbations at a critical radius. The experimental points obtained with the isothermal boundary layer indicate a critical Reynolds Number close to 380, while the refrigerated boundary layer presents lower critical values (336). This reduction is quite impressive, considering that the refrigeration of the disk produced rather moderate viscosity variations in the boundary layer.

For the sake of comparison of the perturbations, we now present the neutral curves of stationary disturbances, for constant viscosity fluids and for fluids with the steady viscosity profile, already given by Pontes *et al.* (2002b, 2003). These curves are presented in Fig. 8 and the destabilizing effect of the steady viscosity profile is clear.

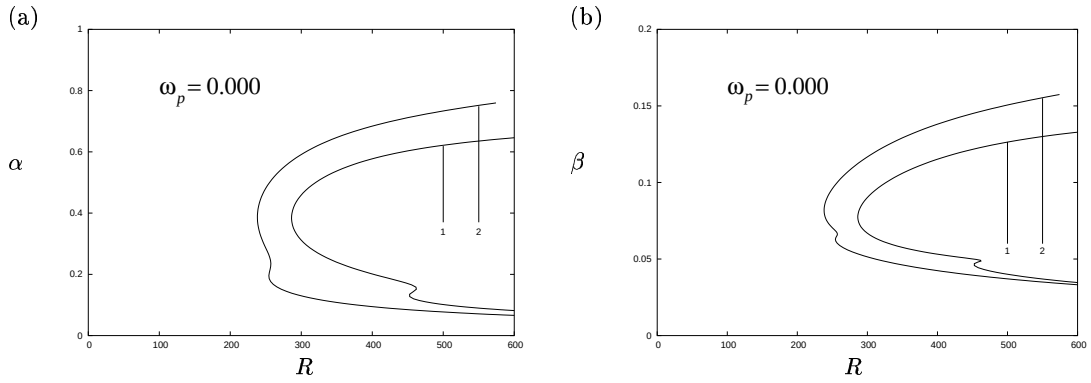

Fig. 8: Neutral curves in the $R \times \alpha$ and $R \times \beta$ planes for stationary disturbances ($\Re(\omega) = 0$) in constant viscosity flows (curves No. 1) and variable viscosity fluids (curves No. 2) with $\nu(0)/\nu(\infty) = 6.0$ and $q = 2.00$ (see Eq. 12).

Comparing the results obtained in the visualization experiments with the results of the linear stability analysis of stationary pertubatons, we can conclude that the two results are in agreement.

7. Conclusions

In conclusion we present an experimental apparatus to corroborate the previous stability analysis of Pontes *et al.* (2002a, 2002b, 2002c, 2003) of rotating disk flows in electro-chemical cells, where the fluid viscosity varies along the axis of the rotating electrode. Previous analysis did not take into account the coupling between the viscosity (temperature) and the hydrodynamic fields, so this work also provides an insight on the results of this coupling.

8. Acknowledgments

J. P. acknowledges financial support received from FAPERJ (Brazil) under the contract number E-26/171.300/2001. N. M. acknowledges financial support received from CNPq. M. B. acknowledges financial support received from UERJ.

9. References

Barcia, O. E., Mattos, O. R., and Tribollet, B., 1992, Anodic dissolution of iron in acid sulfate under mass transport control, "J. Eletrochem. Soc.", Vol. 139, pp. 446–453.

Faller, A. J., 1991, Instability and Transition of the Disturbed Flow Over a Rotating Disk, "J. Fluid Mech.", Vol. 230, pp. 245–269.

Ferreira, J. R. R. M., Barcia, O. E., and Tribollet, B., 1994, Iron dissolution under mass transport control: the effect of viscosity on the current oscillation, "Eletrochim. Acta", Vol. 39, pp. 933–938.

Lingwood, R. J., 1995, Absolute instability of the boundary layer on a rotating disk, "J. Fluid Mech.", Vol. 299, pp. 17–33.

Malik, M. R., 1986, The Neutral Curve for Stationary Disturbances in Rotating-disk Flow, "J. Fluid Mech.", Vol. 164, pp. 275–287.

Pontes, J., Mangiavacchi, N., Conceição, A. R., Barcia, O. E., Mattos, O. E., and Tribollet, B., 2002a, Instabilities in Electrtochemical Systems with a Rotatinng Disk electrode, "J. of the Braz. Soc. of Mechanical Sciences", Vol. XXIV-3, pp. 139–148.

Pontes, J., Mangiavacchi, N., Conceição, A. R., Barcia, O. E., Mattos, O. R., and Tribollet, B., 2002b, Hydrodynamic Stability in an Electrochemical Cell with a Rotating Disk Electrode, "Proceedings of the 9^{th} Brazilian Congress of Thermal Engineering and Sciences", Caxambu, MG, Brazil. paper CIT02-0125 (in CD).

Pontes, J., Mangiavacchi, N., Conceição, A. R., Barcia, O. E., Mattos, O. R., and Tribollet, B., 2002c, Rotating Disk Flow Stability in Eletrochemical Cells, "Anais da III Escola Brasileira de Primavera Transição e Turbulência", Florianópolis, SC, Brazil. (in CD).

Pontes, J., Mangiavacchi, N., Conceição, A. R., Barcia, O. E., Mattos, O. R., and Tribollet, B., 2003, Rotating Disk Flow Stability in Electrochemical Cells: Effect of Fluid Viscosity, submitted, Phys. Fluids.

Schlichting, H. and Gersten, K., 2000, "Boundary Layer Theory", Springer.

von Kármán, T. and Angew, Z., 1921, Uber Laminare und Turbulente Reibung, "Math. Mec.", Vol. 1, pp. 233–252.